Modeling of deformations of photolithographic objects.

A. Touati, Serge Corbel, Jean-Pierre Corriou

Modeling of deformations of photolithographic objects

A. Touati[a], S. Corbel[a] and J.P. Corriou[b*]
[a] DCPR-CNRS-ENSIC-INPL
[b]LSGC-CNRS-ENSIC-INPL , 1 rue Grandville , BP 20451 54001 Nancy Cedex

Abstract

Photolithography allows the fabrication of a solid polymer object through polymerization of a monomer resin by means of a laser source guided according to the data of computer aided design. However, one drawback of this method is the inaccuracy of the dimensions of the objects related to the shrinkage phenomenon which depends on the polymerization, on the laser flux and on the used sweeping procedure. In this paper, the deformation of an isolated voxel (elementary volume) or a voxel interacting with its neighbor is described. This simulation is based on a kinetic model that takes into account the gel effect and a model of volumetric variation due to the difference of the length of the bonds between the monomer and polymer molecules.

Keywords

Photolithography, polymerization, shrinkage, prototyping

1 Introduction

The techniques of fast prototyping nowadays [1] meet a large industrial success for the fabrication of prototype objects [2, 3]. Among them, photolithography [4, 5] which is based on space photopolymerization of a monomer resin [6] is a process that suffers from drawbacks such as shrinkage and aging [7]. The shrinkage is related to the liquid-solid transformation and induces a contraction of the irradiated volume. This contraction is not homogeneous and consequently gives rise to internal stresses which themselves provoke a deformation of the final object. To remedy to that problem, two main directions of research have been studied. The first one consists in acting on the material by using a resin with a low shrinkage [8, 9, 10], a resin charged by a rigid material or a powder suspension in a liquid resin [11]. In the second manner, the system is directly influenced and especially new motives of filling the layers are used [12, 13] in order to reduce the deformations. This latter solution needs the understanding of the kinetics of shrinkage and deformation. In this study, the deformation of an isolated voxel (elementary volume) or a voxel interacting with its neighbor is described. A model of the photopolymerization reaction taking into account the gel effect and a quantitative model based on the previous one to describe the volumetric shrinkage of the polymer constitute the total model used in the simulation.

*e-mail: corriou@ensic.inpl-nancy.fr

2 Model of the polymerization kinetics

During a photopolymerization, the variation of the irradiated volume follows a sigmoidal curve when the resin is irradiated by a light of convenient photonic energy (Fig. 1). It is composed of three zones:

- the first one, where the volume varies slowly, corresponds to the start of the reaction, consumption of the inhibitors, creation of active sites ...,
- the second one, where the volume varies rapidly, is linked to the polymerization in a medium which is still liquid,
- the third one, where the volume is nearly constant, corresponds to the reticulation which leads to a material strictly insoluble in the liquid resin.

The kinetics of such a reaction can be schematically represented according to the following mechanism [14, 15, 16]

photochemical initiation	$A + h\nu \xrightarrow{I_a\phi} 2R^\bullet$		(1)
propagation of "'type 1"	$R^\bullet + M \xrightarrow{k_1} P_1^\bullet$	ΔV_0	(2)
	$P_1^\bullet + M \xrightarrow{k_1} P_1^\bullet$	ΔV_0	(3)
	$P_1^\bullet + P_1^\bullet \xrightarrow{k_1} P_2^\bullet$	ΔV_1	(4)
propagation of "'type 2"	$P_2^\bullet + P_1^\bullet \xrightarrow{k_2} P_1^\bullet$	ΔV_1	(5)
	$P_2^\bullet + M \xrightarrow{k_2} P_2^\bullet$	ΔV_0	(6)
	$P_2^\bullet + P_2^\bullet \xrightarrow{k_2} P_2^\bullet$	ΔV_2	(7)
	$P_2^\bullet + P_1^\bullet \xrightarrow{k_2} P_n^\bullet$	ΔV_2	(8)
	$P_2^\bullet + P_2^\bullet \xrightarrow{k_2} P_n^\bullet$	ΔV_2	(9)
propagation of "'type 3"	$P_n^\bullet + M \xrightarrow{k_3} P_n^\bullet$	ΔV_0	(10)
termination	$P_1^\bullet + P_1^\bullet \xrightarrow{k_1} N$	ΔV_0	(11)
	$P_2^\bullet + P_2^\bullet \xrightarrow{k_2} N$	ΔV_2	(12)
	$P_n^\bullet + P_n^\bullet \xrightarrow{k_3} N$	ΔV_2	(13)

It is assumed that the chemical reactivity of the macroradicals (having the same number of active sites) is practically the same whatever the chain length, i.e. they are kinetically indiscernible.

In all the stages of "type 1" propagation, the macroradicals have a single active center. We consider that the reaction constants are equal to k_1. For the stages of "type 2" propagation, the macroradicals have two active centers and consequently, they are more reactive than those of "type 1". Their kinetic constants k_2 are equal and arbitrarily fixed at $10k_1$. In the stages of "type 3" propagation, the macroradicals have more than two active centers and the kinetic constant k_3 is similarly taken as $100k_2$.

2.1 Kinetic model

The kinetic model corresponding to the previous reaction mechanism is composed by the following differential equations

$$\frac{d[R^\bullet]}{dt} = I_a\phi - k_1\,[R^\bullet]\,[M] \tag{14}$$

$$\frac{d[M]}{dt} = -k_1\,[R^\bullet]\,[M] - k_1\,[P_1^\bullet]\,[M] - k_2\,[P_2^\bullet]\,[M] - k_3\,[P_3^\bullet]\,[M] \tag{15}$$

$$\frac{d[P_1^\bullet]}{dt} = k_1\,[R^\bullet]\,[M] - 4\,k_1\,[P_1^\bullet]^2 - k_2\,[P_1^\bullet]\,[P_2^\bullet] \tag{16}$$

$$\frac{d[P_2^\bullet]}{dt} = k_1\,[P_1^\bullet]^2 - 2\,k_2\,[P_1^\bullet]\,[P_2^\bullet] - 5\,k_2\,[P_2^\bullet]^2 \tag{17}$$

$$\frac{d[P_n^\bullet]}{dt} = k_2\,[P_1^\bullet]\,[P_2^\bullet] + k_2\,[P_2^\bullet]^2 - 2\,k_3\,[P_n^\bullet]^2 \tag{18}$$

2.1.1 Kinetic constants of the reactions

The considered model takes into account the gel effect, i.e. the confining of the reactive species in the reacting medium and consequently the limitation of the conversion rate. An apparent kinetic constant equal to

$$K_i = \frac{k_i\,k_D}{k_i + k_D} \qquad i = 1, 2, 3 \tag{19}$$

has been used for each reaction stage where k_i is a kinetic propagation constant following Arrhenius law

$$k_i = k_i^0 \exp\left(\frac{-E_i}{RT}\right) \tag{20}$$

and k_D a term for the diffusion of molecules in the medium [17]

$$k_D = 2.2\ 10^6\ \frac{T}{\eta} \tag{21}$$

with T temperature of the medium (K), R gas constant (J.mol^{-1}.K^{-1}), E_i propagation activation energy (J.mol^{-1}), η viscosity of the medium (Pa.s).

At the beginning of the reticulating photopolymerization reaction, the system is liquid (more or less viscous according to its nature), then it transforms itself into a transient gel state and finally, in a rapid way, into a dense solid. An approximate expression of the medium viscosity [14] which takes into account the change of state: liquid → gel → solid, is

$$\eta = \eta_0\ \exp\left(\frac{\chi}{\chi_\infty - \chi}\right) \tag{22}$$

with χ the conversion rate of the monomer and χ_∞ the final conversion rate.

Experimentally, the conversion rate for a diacrylic monomer does not exceed 60 or 70% due to the capturing of the macroradicals which can no more react. When χ tends towards 0.6, the viscosity tends towards a very large value (fixed as a finite value in the model simulation, 10^9 Pa.s). When η is expressed with respect to the number of monomer units $x_m(t)$ remaining at time t in the reaction medium, it gives

$$\eta = \eta_0 \exp\left[\lambda\left(\frac{1}{x_m(t)} - \frac{1}{x_m(t_0)}\right)\right] \tag{23}$$

with $\eta_0 = 10^{-3}$ Pa.s, λ is a constant such that $\eta = 10^9$ Pa.s when $\chi = 0.6$ and $x_m(t_0)$ is the initial number of monomer units.

2.1.2 Relation between the intensity of the absorbed light and the depth of polymerization

The intensity I_t transmitted through an absorbing medium follows Beer-Lambert law

$$I_t(z) = I_0\ \exp(-\epsilon_\lambda c z) \tag{24}$$

with I_0 intensity of the incident flux, ϵ_λ extinction coefficient at wavelength λ, c concentration in absorbing species and z thickness of the medium.

The light intensity absorbed by an elementary layer of thickness dz at depth z is

$$I_{a,z}(dz) = -dI_t(z) = \epsilon_\lambda \, c \, I_0 \; \exp(-\epsilon_\lambda \, c \, z) \, dz \tag{25}$$

If an elementary volume (voxel) which is a square parallelepiped is subdivided into n_{max} layers of thickness Δz (Fig. 1) and if the absorption is supposed to be homogeneous in each layer, the absorbed flux in the n^{th} layer is

$$I_{abs} = I_0 \; \{\exp\left[-\epsilon_\lambda \, c \, (n-1) \, \Delta z\right] - \exp\left[-\epsilon_\lambda \, c \, n \, \Delta z\right]\} \tag{26}$$

In order to eliminate the factor $(\epsilon_\lambda \, c)$ related to the initiator, a transmission rate $\tau_{z,trans}$ equal to the ratio between the incident intensity and that transmitted at depth z_0, with z_0 total thickness of the sample is defined

$$\tau_{z,trans} = \frac{I_t(z_0)}{I_0} = \exp(-\epsilon_\lambda \, c \, z_0) \tag{27}$$

with

$$z_0 = -\frac{\ln(\tau_{z,trans})}{\epsilon_\lambda \, c} = n_{max} \, \Delta z \tag{28}$$

from which the intensity absorbed by a layer n results

$$I_{abs} = I_0 \left\{ \exp\left[\frac{n-1}{n_{max}} \ln(\tau_{z,trans})\right] - \exp\left[\frac{n}{n_{max}} \ln(\tau_{z,trans})\right] \right\} \tag{29}$$

with I_0 and I_{abs} in E.mm^{-2}.s^{-1} (E : Einstein).

2.2 Simulation results

The numerical data [14] have been used for simulation are given in Table 1.

Table 1: Numerical data for simulation

$x_m(t_0) = 200$	$\tau_{z,trans} = 0.01$
$I_0 = 3.10^{-7}$ E.mm^{-2}.s^{-1}	$\phi = 0.5$ mol.E^{-1}
$l_0 = 1$ mm	$k_1^0 = 8.7 \; 10^5$ l.mol^{-1}.s^{-1}
$z_0 = 0.5$ mm	$E_1 = 4.7$ J.mol^{-1}
$n_{max} = 10$	$R = 8.314$ J.mol^{-1}.K^{-1}

The results, presented on Figure 2, show the variation of the monomer conversion with respect to time for the different layers. It can be noticed that these layers have an inflexion all the more pronounced as the layer is close to the free surface of the resin, which is consistent with physics laws. On the other side, each curve has a sigmoidal shape: the reaction of the molecules is slow at the beginning than it becomes faster due to the reticulation of the medium (several sites are active), then it decreases because of the macroradicals which are enclosed.

3 Model of the volumetric variation

The transformation monomer-polymer is accompanied by a decrease of the irradiated volume or volumetric shrinkage which follows a sigmoidal curve (Fig. 3). The model described by Fig. 1 has been used to represent it.

3.1 Volumetric model

The principal of the simulation model is the following: a variation of the elementary volume is associated to each stage of the kinetic model given by equations (1) to (13), this variation depends on the size of the reacting molecules. A small volumetric variation ΔV_0 is associated to the conversion of the monomer molecules, a large volumetric variation ΔV_1 is associated to the macroradicals having a single active center, and a larger volumetric variation ΔV_2 is associated to the macroradicals having more than one active center (the volumetric variation due to reticulation increases with the number of active centers). The volumetric variation for each reaction stage is determined in the following manner: the time derivative of the volume times the sum of the concentrations of the different reactive species figuring in the equation of the reaction stage is equal to the product of the rate of that stage by the elementary volumetric variation. This calculation results in

$$\text{Stage (1)} \qquad -[M]\,\frac{dV}{dt} = k_1\,[R^\bullet]\,[M]\,\Delta V_0 \tag{30}$$

$$\text{Stage (2)} \qquad -[M]\,\frac{dV}{dt} = k_1\,[P_1^\bullet]\,[M]\,\Delta V_0 \tag{31}$$

$$\text{Stage (3)} \qquad ([P_2^\bullet] - 2\,[P_1^\bullet])\,\frac{dV}{dt} = k_1\,[P_1^\bullet]^2\,\Delta V_1 \tag{32}$$

$$\text{Stage (4)} \qquad -[P_2^\bullet]\,\frac{dV}{dt} = k_1\,[P_1^\bullet]\,[P_2^\bullet]\,\Delta V_1 \tag{33}$$

$$\text{Stage (5)} \qquad -[M]\,\frac{dV}{dt} = k_2\,[P_2^\bullet]\,[M]\,\Delta V_0 \tag{34}$$

$$\text{Stage (6)} \qquad -[P_2^\bullet]\,\frac{dV}{dt} = k_2\,[P_2^\bullet]^2\,\Delta V_2 \tag{35}$$

$$\text{Stage (7)} \qquad ([P_n^\bullet] - [P_1^\bullet] - [P_2^\bullet])\,\frac{dV}{dt} = k_2\,[P_1^\bullet]\,[P_2^\bullet]\,\Delta V_2 \tag{36}$$

$$\text{Stage (8)} \qquad ([P_n^\bullet] - 2\,[P_2^\bullet])\,\frac{dV}{dt} = k_2\,[P_2^\bullet]^2\,\Delta V_2 \tag{37}$$

$$\text{Stage (9)} \qquad -[M]\,\frac{dV}{dt} = k_3\,[P_n^\bullet]\,[M]\,\Delta V_0 \tag{38}$$

$$\text{Stage (10)} \qquad -2\,[P_1^\bullet]\,\frac{dV}{dt} = k_1\,[P_1^\bullet]^2\,\Delta V_0 \tag{39}$$

$$\text{Stage (11)} \qquad -2\,[P_2^\bullet]\,\frac{dV}{dt} = k_2\,[P_2^\bullet]^2\,\Delta V_2 \tag{40}$$

$$\text{Stage (12)} \qquad -2\,[P_n^\bullet]\,\frac{dV}{dt} = k_3\,[P_n^\bullet]^2\,\Delta V_2 \tag{41}$$

The total volumetric variation results

$$\begin{aligned} -\frac{dV}{dt} = \;& k_1\,[R^\bullet]\,\Delta V_0 + k_1\,[P_1^\bullet]\,\Delta V_0 + \frac{k_1\,[P_1^\bullet]^2}{2\,[P_1^\bullet] - [P_2^\bullet]}\,\Delta V_1 + k_1\,[P_1^\bullet]\,\Delta V_1 + k_2\,[P_2^\bullet]\,\Delta V_0 \\ & + k_2\,[P_2^\bullet]\,\Delta V_2 + \frac{k_2\,[P_1^\bullet]\,[P_2^\bullet]}{[P_1^\bullet] + [P_2^\bullet] - [P_n^\bullet]}\,\Delta V_2 + \frac{k_2\,[P_2^\bullet]^2}{2\,[P_2^\bullet] - [P_n^\bullet]}\,\Delta V_2 \\ & + k_3\,[P_n^\bullet]\,\Delta V_0 + \tfrac{k_1}{2}\,[P_1^\bullet]\,\Delta V_0 + \tfrac{k_2}{2}\,[P_2^\bullet]\,\Delta V_2 + \tfrac{k_3}{2}\,[P_n^\bullet]\,\Delta V_2 \end{aligned} \tag{42}$$

Let us assume that the elementary volumetric variations ΔV_1 and ΔV_2 are proportional to ΔV_0 as

$$\Delta V_1 = \beta_1\,\Delta V_0 \qquad \text{and:} \qquad \Delta V_2 = \beta_2\,\Delta V_0 \tag{43}$$

where β_1 and β_2 are coefficients estimated by an optimization procedure so as to minimize the deviation between the simulated curves $\Delta V/V = f(t)$ and the experimental data. The analytical expression of ΔV_0 can be obtained in the following manner: as the final volume V_{fin} of the polymerized sample is known, it is possible to define a shrinkage rate α_{max} such that

$$V_{fin} - V_0 = -\alpha_{max}\,V_0 \tag{44}$$

with V_0 initial volume of the monomer. At time t, the volume of the sample is

$$V(t) = \int_0^t \frac{dV}{dx} dx + V_0 \tag{45}$$

such that, at the end of reaction at time t_{fin}, the volumetric variation is given by equation (44). The following approximation of the integral can be performed

$$\sum_{i=0} N \left(\frac{\Delta V}{\Delta t}\right)_i \Delta t_{int} \approx -\alpha_{max} V_0 \tag{46}$$

with i such that $t_i = i\Delta t_{int}$, Δt_{int} the time integration step and $t_{fin} = N\Delta t_{int}$. The relative volumetric variation can be formulated for interval $[t_i, t_i + \Delta t_{int}]$ as

$$\left(\frac{\Delta V}{\Delta t}\right)_i = -f_0(t_i)\,\Delta V_0 - f_1(t_i)\,\Delta V_1 - f_2(t_i)\,\Delta V_2 = -[f_0(t_i) + \beta_1\, f_1(t_i) + \beta_2\, f_2(t_i)]\,\Delta V_0 \tag{47}$$

where $f_0(t_i)$, $f_1(t_i)$ and $f_2(t_i)$ depend on the concentrations of the active species of the medium at time ti. The total volumetric variation results

$$\sum_{i=0}^{N} \left(\frac{\Delta V}{\Delta t}\right)_i \Delta t_{int} \approx -\Delta V_0\, \Delta t_{int} \sum_{t_i=0}^{t_{fin}} [f_0(t_i) + \beta_1\, f_1(t_i) + \beta_2\, f_2(t_i)] \tag{48}$$

hence

$$\Delta V_0 \approx \frac{\alpha_{max}\, V_0}{\Delta t_{int} \sum\limits_{t_i=0}^{t_{fin}} [f_0(t_i) + \beta_1\, f_1(t_i) + \beta_2\, f_2(t_i)]} \tag{49}$$

Thus the value of ΔV_0 depends on two experimental parameters V_0 and α_{max} and on both parameters of the volumetric variation β_1 and β_2.

3.2 Simulation results

The relative volumetric variation with respect to time is represented on Figure 4 (for $\beta_1 = \beta_2 = 1$) and Figure 5 (for $\beta_1 = 10$ and $\beta_2 = 100$). The choice of the values of β_1 and β_2 is arbitrary and its objective is to study the effect of these parameters on the volumetric shrinkage. The numerical data are the same as those used in section 2.3 with $\alpha_{max} = 0.15$. The curves have the same shape in both cases but the volumetric decrease is more important in the second case. Indeed, only five stages (equations (30), (31), (34), (38) and (39)) among the twelve composing the kinetic model lead to a variation ΔV_0 (due to a transformation of the monomer) and moreover, as the reaction progresses, the monomer is consumed.

4 Model of a vortex deformation

4.1 Description of the geometrical simulation

Assume that the laser ray has a square cross section of side 1 mm and that it is perpendicular to the monomer surface. Thus the polymerized voxel has a cross section of 1 mm^2 and a depth z_0. In the simulation model, the voxel is divided into n_{max} layers of thickness Δz at $t = 0$ (Fig. 6), the evolution of the thickness of each layer is calculated from the volumetric variation presented on Fig. 4. It is assumed that each layer can freely slip with respect to the other. At time t, each layer n is described by its length $l(n,t)$ and its thickness $e(n,t)$. The linear shrinkage coefficient $k_r(n,t)$ of the n^{th} layer at time t is defined by $l(n,t) = k_r(n,t)l_0$ and $e(n,t) = k_r(n,t)\Delta z$, thus the volume $v(n,t)$ of the n^{th} layer is

$$v(n,t) = e(n,t)\, l^2(n,t) = k_r^3(n,t)\, l_0^2\, \Delta z \tag{50}$$

Being given that the initial volume v_0 of a layer at $t = 0$ is: $v_0 = l_0^2 \, \Delta z$, then the linear shrinkage coefficient $k_r(n,t)$ is

$$k_r(n,t) = \left(\frac{v(n,t)}{v_0} \right)^{\frac{1}{3}} \tag{51}$$

and the depth of the layer n is

$$z(n,t) = \sum_{i=1}^{n} e(i,t) \tag{52}$$

with $z_0 = z(n_{max}, 0) = n_{max} \Delta z$.

The set of equations describing the layer n at time t is

$$\begin{cases} l(n,t) = k_r(n,t) \, l_0 \\ z(n,t) = \frac{z_0}{n_{max}} \sum_{i=1}^{n} k_r(i,t) \\ e(n,t) = k_r(n,t) \, \Delta z \end{cases} \tag{53}$$

The origin of the vertical axis Oz is the free surface of the resin and the axis Oz is oriented downwards. It is assumed that the top of the voxel remains at $z = 0$, thus the shrinkage occurs for $z > 0$. If the polymerization is independent of any physical constraint (such as gravity forces), the description of the deformation of the voxel section is relatively simple. In the present simulation, the voxel is assumed to adhere to the reactor wall.

4.2 Simulation results

The numerical data used in the simulation of the volumetric variation of a voxel during polymerization are gathered in Tab. 2 where Δt is the time of irradiation of a voxel.

Table 2: Numerical data for the volumetric variation

$l_0 = 1$ mm	$z_0 = 0.5$ mm
$\Delta z = 0.05$ mm	$n_{max} = 10$
$\Delta t = 0.1$ s	$\alpha_{max} = 0.15$
$\tau_{z,trans} = 0.01$	$I_0 = 3 \; 10^{-7}$ E.mm^{-2}.s^{-1}

The deformation of the right half-part of the voxel has been simulated as the deformation is symmetrical with respect to its axis. On Fig. 7, the deformation of a voxel after 0.1 s irradiation is represented during polymerization. It appears that the voxel shrinks with respect to the horizontal and vertical directions, inducing a decrease of its length and thickness. This decrease is more important for the layers closer to the surface which absorb more laser flux (according to Beer-Lambert law).

5 Model of an element of two voxels

5.1 Description of the deformation of two adjacent voxels

At time $t = 0$, the laser light starts the sweeping of the first voxel on the surface of the resin. The sweeping of a line of polymer is described by Fig. 8. Δt is the irradiation time for a voxel. The first irradiated voxel is the one adhering to the reactor wall, then at each period Δt, the adjacent voxel is irradiated to produce the line formed by n_{vox} voxels.

From time $t = 0$ to $t = \Delta t$, the first voxel starts shrinking and deforming itself as indicated at the previous section. At time $t = \Delta t$, the angle between the layer and the vertical is α_1 (Fig. 9). This angle is negative as the chosen positive direction is clockwise. Then, at $t = \Delta t$, the irradiation of the second voxel starts. It is assumed that this second voxel starts shrinking independently of the first one, and a fictitious angle α_2 is defined (Fig. 10) between the left side of the first layer of the second voxel with vertical if it shrinks freely; again only one side is concerned as the shrinkage is assumed to be symmetrical. However, the second voxel follows the deformation of the first one and has its own volumetric variation. The global deformation of the second voxel is characterized by the angle α_g between its first layer and horizontal

$$\alpha_g = \alpha_1 + \alpha_2 \tag{54}$$

the second voxel deformates itself upwards if $\alpha_g < 0$ and downwards if $\alpha_g > 0$ (Fig. 11). Let us calculate the angle $\alpha_g(1,t)$ of the first layer of the second voxel with horizontal at time t

$$\alpha_g(1,t) = \alpha_1(1,t) + \alpha_2(1,t-\Delta t) \tag{55}$$

with $\alpha_1(1,t)$ related to the first voxel, such that

$$\tan(\alpha_1(l,t)) = \left| \frac{l(i,t) - l(2,t)}{2e(1,t)} \right| \tag{56}$$

where $l(1,t)$ and $l(2,t)$ are the lengths of the first and second layers, $e(1,t)$ is the thickness of the first layer at time t. The value of α_2 derives from the following equation

$$\tan(\alpha_2(l,t-\Delta t)) = \left| \frac{l(i,t-\Delta t) - l(2,t-\Delta t)}{2e(1,t-\Delta t)} \right| \tag{57}$$

These hypotheses, i.e. the deformation of the second voxel follows that of the first one and the angle α_g of the first layer of the second voxel with horizontal influences the global deformation of the second voxel, require that each voxel remains sufficiently flexible to be able to follow the deformation of the adjacent voxel, but simultaneously sufficiently solid to deformate itself as a single object. Thus, any voxel must remain viscous during all the simulation of the deformation of the element.

5.2 Simulation results

The deformation of an element formed by two adjacent voxels was simulated with the same numerical data as Tab. 2 and a sweeping velocity $v_s = 10$ mm.s^{-1}. Fig. 11 represents the result of that simulation at different times. A value of α_{max} (0.15) larger than the experimental value (0.10) [14] was used to amplify the deformations and emphasize the behavior of a voxel during polymerization.

It can be noticed that the deformation of the bar is the result of the deformations of each voxel as well as of the interaction between both of them. This makes the accumulation of the deformations in an irradiated line clear, which is in agreement with the experimental result found by [18, 19]. It shows that the use of a single line by segmentation of the swept lines improves the final state of the beam produced by photolithography.

The method used to simulate the deformation of two adjacent voxels can be generalized to analyze the deformation of a beam formed by n_vox voxels. The shrinkage of the $(i+1)^{th}$ voxel is delayed by Δt (sweeping time for one voxel) with respect to that of the previous adjacent voxel with respect to the sweeping. Therefore the data describing the voxel $i+1$ at time t are the same as those of the voxel i at time $t - \Delta t$. Thus, to record the deformation at time t of a beam of n_{vox} voxels, it suffices only to have the data describing one voxel at successive times $t - (n_{vox} - 1)\Delta t, \ldots, t - \Delta t, t$. The variation of the profile of the beam with respect to time is characterized by the propagation of a vertical deformation, related to angle α_g, in the sweeping direction. The voxels that are deformed at a given time stand up again at the following times. If the beam is assumed to remain sufficiently soft, it stands up again totally by itself when time progresses. However, the polymer becomes more rigid with time and the relaxation of the beam becomes less obvious.

6 Conclusion

In this paper, a model of simulation of the behavior of an elementary volume of monomer during photopolymerization has been developed. First, a kinetic model of the photopolymerization reaction takes into account the variation of viscosity of the medium. This model has been used to develop the final model dedicated to the simulation of the volumetric shrinkage of each voxel. These simulations show the importance of the gel effect and the difference of behavior of the reactant before and after the gel point. The simulations performed by means of a geometrical model allow us to describe the deformation of an isolated voxel or of a voxel interacting with its neighbor. This simple model describes the relaxation of a line swept by a laser and demonstrates that the deformation accumulates itself with time. The results of that simulation are in agreement with the experimental observations concerning the deformation of a beam: the alternate sweeping avoids the propagation of the deformation (memory effect) and minimizes the interaction between the irradiated elements, i.e. the internal stresses that are generated.

Nomenclature

c	monomer concentration (mol.m^{-3})
$e(n,t)$	thickness of layer n at time t (m)
E	propagation activation energy (J.mol^{-1})
I_a	intensity of the absorbed flux (E.mm^{-3}.s^{-1})
I_t	transmitted intensity (E.mm^{-2}.s^{-1})
I_0	intensity of the incident flux (E.mm^{-2}.s^{-1})
k_1, k_2, k_3	kinetic constant (m^3.mol^{-1}.s^{-1})
k_D	diffusion constant of molecules (m^3.mol^{-1}.s^{-1})
l_0	initial length of one voxel (m)
$l(n,t)$	length of layer n at time t (m)
M	monomer
n	number of a layer
P	polymer
r_t	number of free radicals at time t
$R^{\bullet}$	radical
R	gas constant (J.mol^{-1}.K^{-1})
$v(n,t)$	volume of a layer (m^3)
v_s	sweeping velocity (m.s^{-1})
V	volume of the voxel (m^3)
t	time (s)
$\tau_{z,trans}$	transmission rate
T	temperature (K)
z	thickness of the voxel at time t (m)
$z(n,t)$	thickness of layer n at time t (m)

Greek symbols

α_{max}	maximum shrinkage rate
α_1, α_2	angles between the layer 1 with vertical respectively for voxels 1 and 2 (rd)
α_g	global angle of deformation (rd)
$\alpha_r(n,t)$	linear shrinkage coefficient
ϵ_λ	extinction coefficient at wavelength l (m^2.mol^{-1})
η	viscosity (Pa.s)

ϕ	quantum yield of radical creation
Δt	irradiation time of one voxel (s)
Δt_{int}	integration step (s)
Δz	thickness of a layer (m)

References

[1] P.J. Bartolo, editor. *Virtual modeling and rapid manufacturing*, 2005. 2nd International Conference on advanced research and rapid prototyping, Leiria, Portugal, Taylor & Francis, Leyden, Netherlands.

[2] C.K. Chua, K.F. Leong, and C.C. Kai. *Rapid Prototyping Principles and Applications in Manufacturing*. John Wiley, 1998.

[3] M. Furman, S. Corbel, H. Le Gall, O. Zahraa, and M.Bouchy. Influence of the geometry of a monolithic support on the efficiency of photocatalyst for air cleaning. *Chem. Eng. Sci.*, doi:10.1016/j.ces.2006.12.045 (in press), 2007.

[4] P. Jacobs. *Stereolithography and Other RP&M Technologies: From Rapid Prototyping to Rapid Tooling*. Lavoisier, 1995.

[5] K.F. Leong. *Rapid Prototyping and Manufacturing: Fundamentals of Stereolithography,*. McGraw Hill, New York, 1993.

[6] M.D. Goodner and C.N. Bowman. Development of comprehensive free radical photopolymerization model incorporating heat and mass transfer effects in thick films. *Chem. Eng. Sci.*, 57:887–900, 2002.

[7] L. Flach and R.P. Chartoff. Laser scan rates and shrinkage in stereolithography. In *Proc. of 4th Int. Conf. Rapid Prototyping, Dayton, OH*, 1993.

[8] J.C. André, M. Cabrera, J.Y. Jézéquel, and P. Karrer. French patent n° 88 06 708,, 1988.

[9] J.C. André, M. Cabrera, and P. Karrer. French patent n° 88 15 887,, 1988.

[10] J.C. André, M. Cabrera, and P. Karrer. French patent n° 88 15 402, 1989.

[11] H.C. Chen, S. Corbel, and A. George. Laser induced paste agglomeration: a new process for rapid prototyping. *J. Physique. IV*, 3(7):2193, 1993.

[12] J. Ullett, R. Chartoff, A. Lightman, D. Murphy, and J. Li. Reducing warpage in stereolithography through novel draw styles. In *Proc. of 5th. Conf. Rapid Prototyping, Dayton, OH*, 1994.

[13] O. Dufaud and S. Corbel. Dispositif de déposition de couches de suspension de céramiques appliqué à la stéréolithographie. *Can. J. Chem. Eng.*, 82:986–993, 2004.

[14] A.M. Duclos, J.Y. Jézéquel, and J.C. André. Industrial photochemistry XX. three-dimensional machining with laser: polymer deformation induced by shrinkage phenomena. *J. Photochem. Photobiol. A : Chem.*, 70:285, 1993.

[15] N.A. Dotson, R. Galvan, R.L. Laurence, and M. Tirrell. *Polymerization process modeling*. VCH Publishers, New York, 1996.

[16] N.G. Mc Crum, C.P. Buckley, and C.B. Bucknall. *Principles of polymer engineering*. Oxford University Press, Oxford, 2nd edition, 1997.

[17] J. Brandrup and E.H. Immergut, editors. *Polymer handbook*. Wiley, New York, 1989.

[18] A. Touati. *Analyse du retrait et réduction des déformation en stéréolithographie*. PhD thesis, INPL, Nancy, France, 1998.

[19] A. Touati, S. Corbel, and J.P. Corriou. Réduction des déformation en stéréolithographie. In *6èmes Assises Européennes du Prototypage rapide, Paris*, 1997.

List of Figures

1 Conversion rate of the monomer with respect to time for the different layers (indexed by increasing n with respect to depth) . . . 12
2 Division of the irradiated volume into a finite number of layers (n_{max}) . . . 13
3 Volumetric variation with respect to the irradiation time . . . 14
4 Relative volumetric variation with respect to time with $\beta_1 = \beta_2 = 1$ . . . 15
5 Relative volumetric variation with respect to time with $\beta_1 = 10$ and $\beta_2 = 100$ . . . 16
6 Division of the voxel into n_{max} layers . . . 17
7 Visualization of the deformation of a voxel after 0.1 s of irradiation . . . 18
8 Fabrication of a polymer line . . . 19
9 Deformation of the first voxel . . . 20
10 Result of the deformation with respect to the global angle α_g . . . 21
11 Visualization of the deformation of two adjacent voxels . . . 22

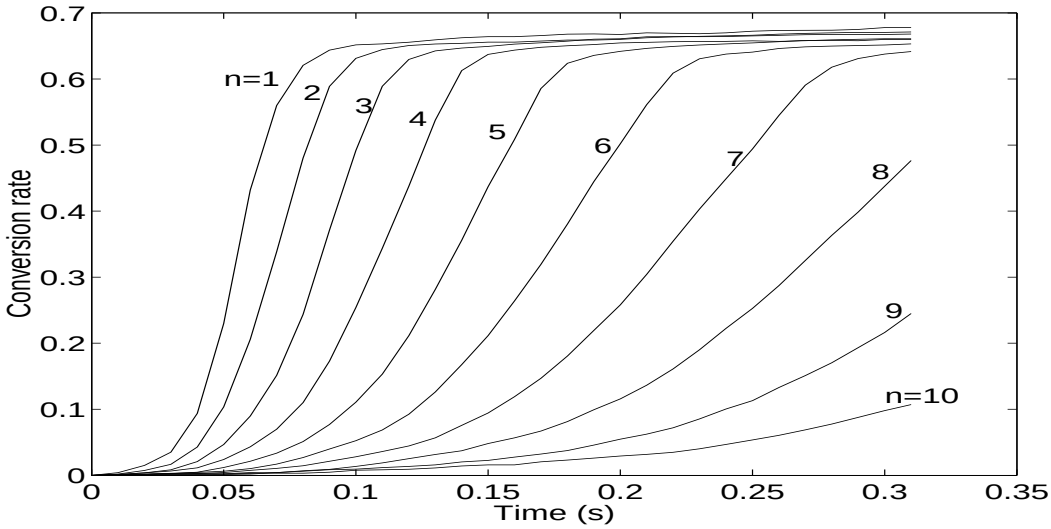

Figure 1: Conversion rate of the monomer with respect to time for the different layers (indexed by increasing n with respect to depth)

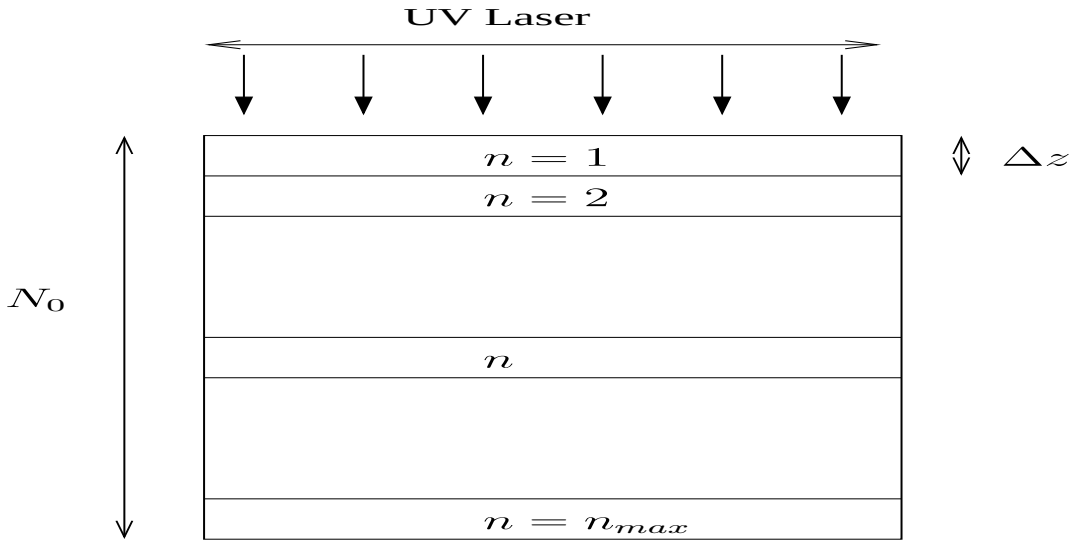

Figure 2: Division of the irradiated volume into a finite number of layers (n_{max})

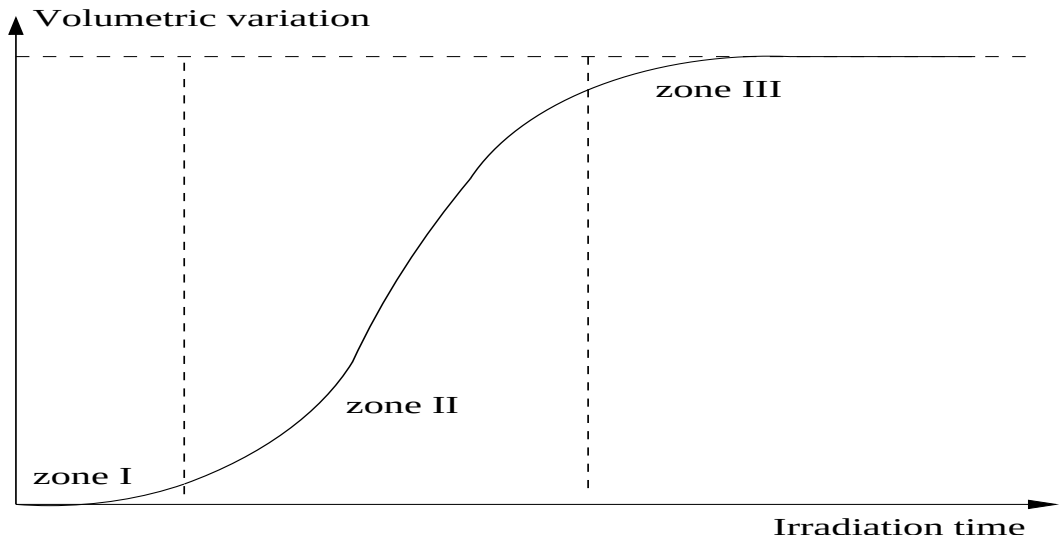

Figure 3: Volumetric variation with respect to the irradiation time

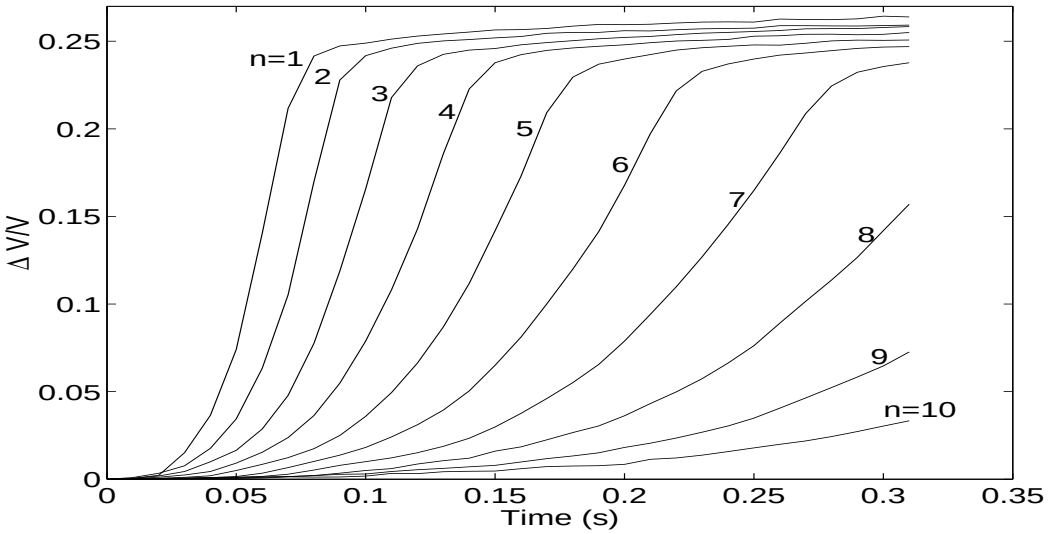

Figure 4: Relative volumetric variation with respect to time with $\beta_1 = \beta_2 = 1$

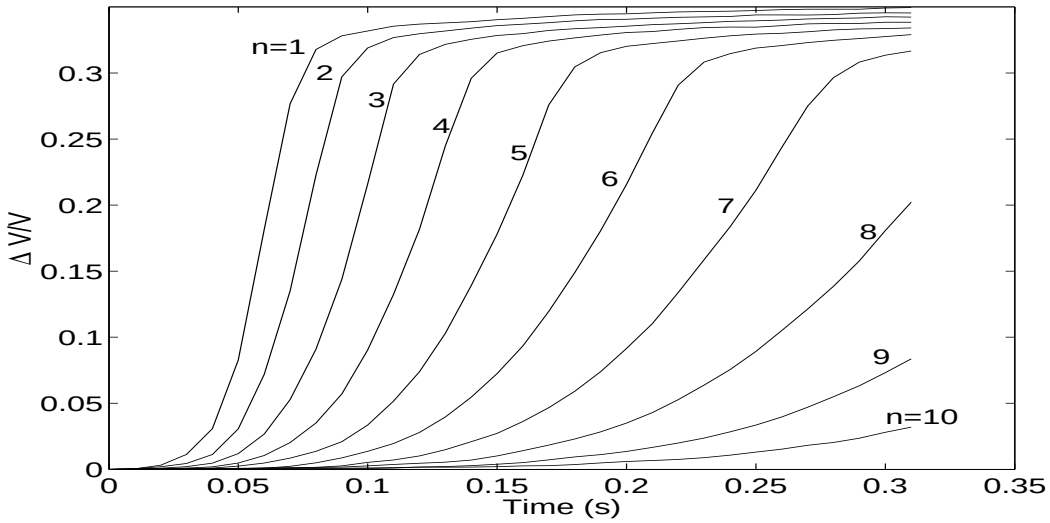

Figure 5: Relative volumetric variation with respect to time with $\beta_1 = 10$ and $\beta_2 = 100$

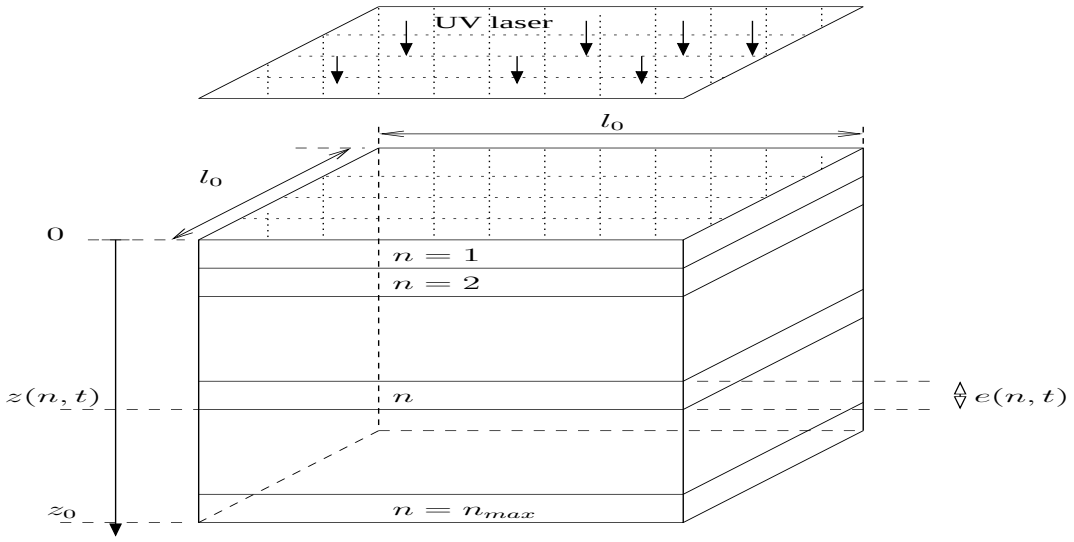

Figure 6: Division of the voxel into n_{max} layers

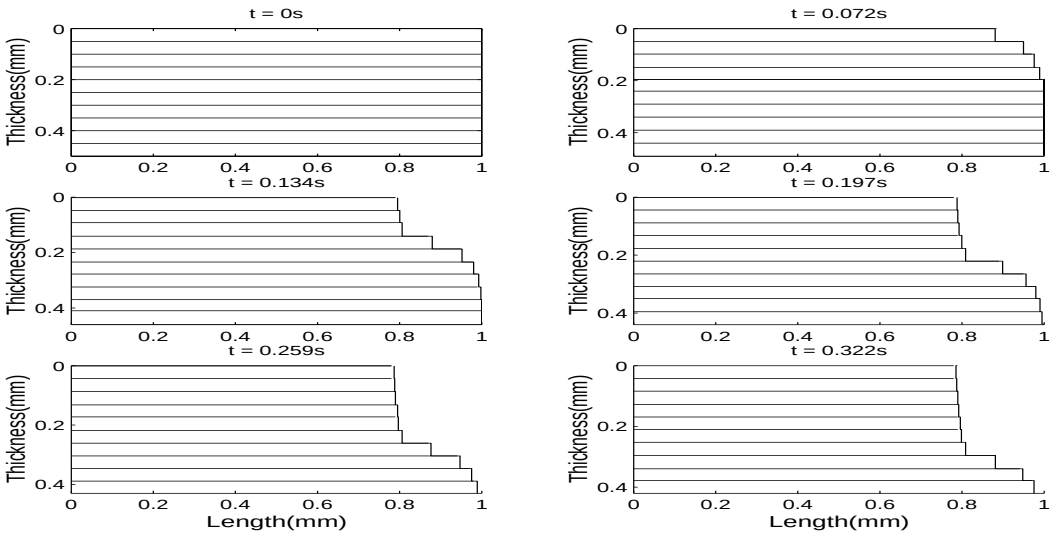

Figure 7: Visualization of the deformation of a voxel after 0.1 s of irradiation

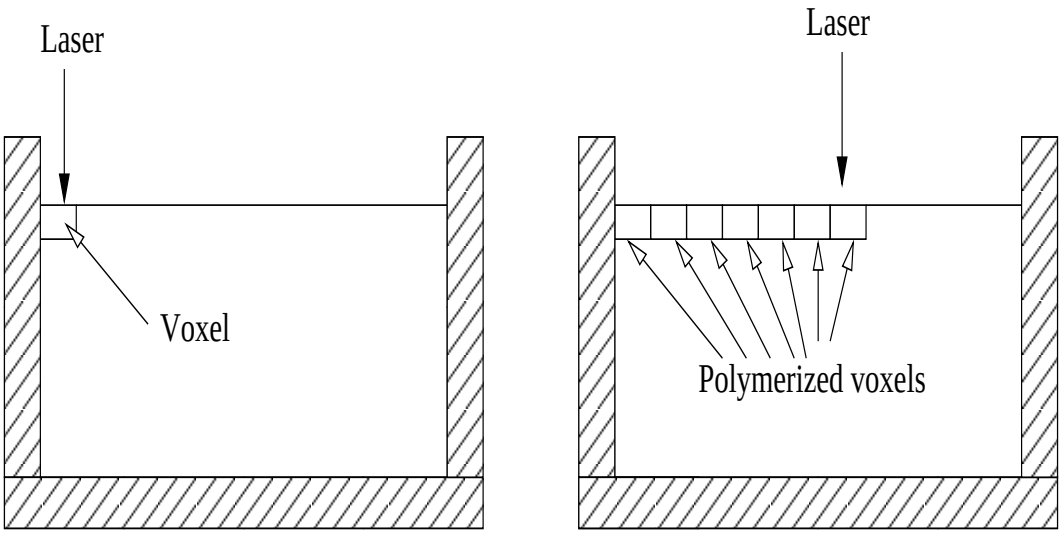

Figure 8: Fabrication of a polymer line

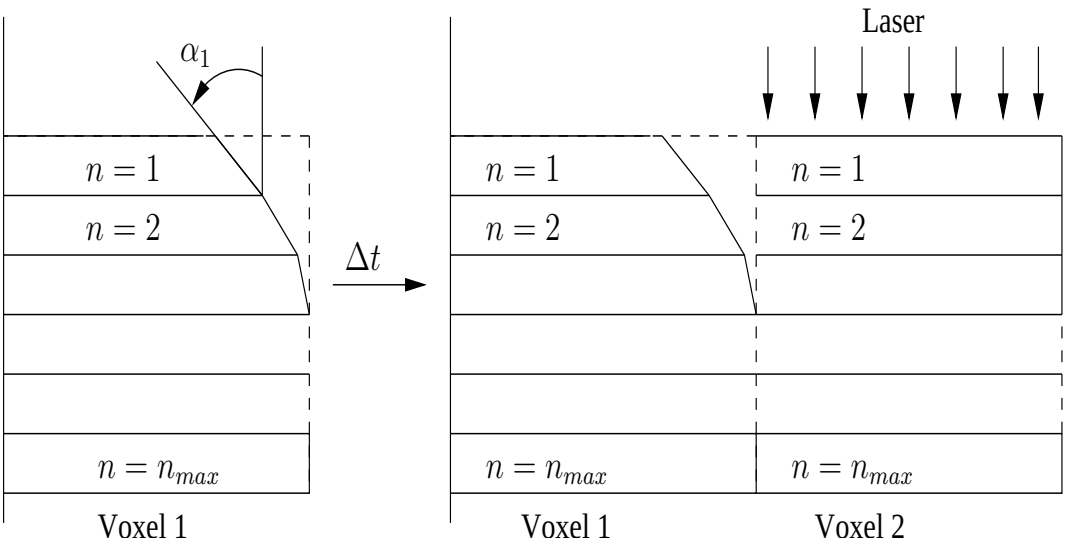

Figure 9: Deformation of the first voxel

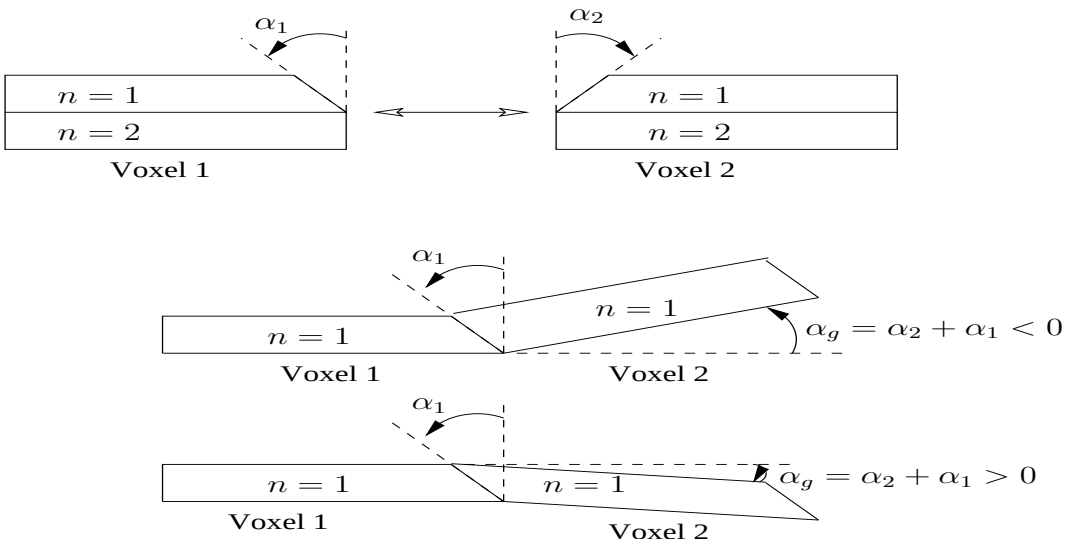

Figure 10: Result of the deformation with respect to the global angle α_g

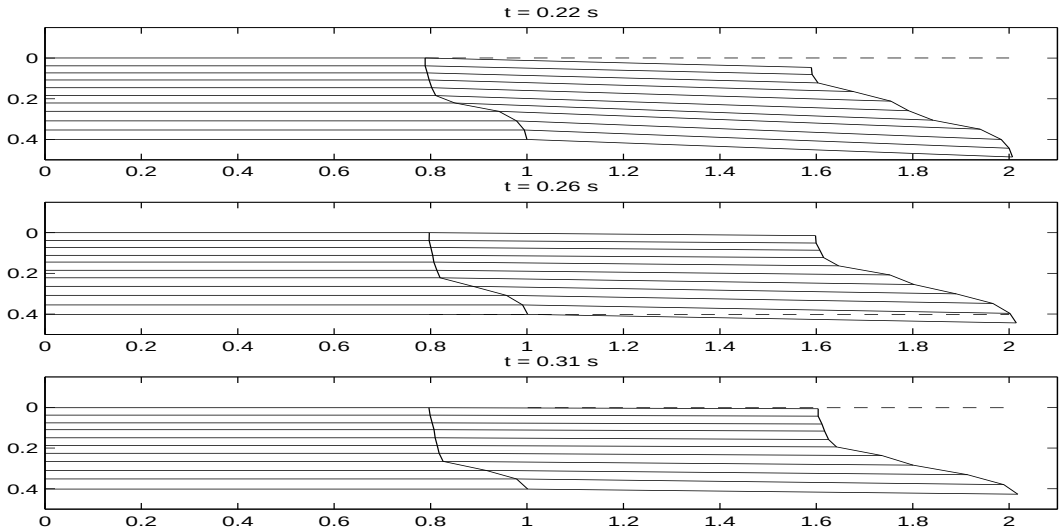

Figure 11: Visualization of the deformation of two adjacent voxels